Breaking the icosahedra in boron carbide

Kelvin Y. Xie[a], Qi An[b], Takanori Sato[c], Andrew J. Breen[c,d], Simon P. Ringer[c,e], William A. Goddard III[b], Julie M. Cairney[c,d], and Kevin J. Hemker[a,f,1]

[a]Department of Mechanical Engineering, Johns Hopkins University, Baltimore, MD 21218; [b]Materials and Process Simulation Center, California Institute of Technology, Pasadena, CA 91125; [c]Australian Centre for Microscopy and Microanalysis, The University of Sydney, Sydney, NSW 2006, Australia; [d]School of Aerospace, Mechanical and Mechatronic Engineering, The University of Sydney, Sydney, NSW 2006, Australia; [e]Australian Institute for Nanoscale Science and Technology, The University of Sydney, Sydney, NSW 2006, Australia; and [f]Department of Materials Science and Engineering, Johns Hopkins University, Baltimore, MD 21218

Edited by William D. Nix, Stanford University, Stanford, CA, and approved August 30, 2016 (received for review May 18, 2016)

Findings of laser-assisted atom probe tomography experiments on boron carbide elucidate an approach for characterizing the atomic structure and interatomic bonding of molecules associated with extraordinary structural stability. The discovery of crystallographic planes in these boron carbide datasets substantiates that crystallinity is maintained to the point of field evaporation, and characterization of individual ionization events gives unexpected evidence of the destruction of individual icosahedra. Statistical analyses of the ions created during the field evaporation process have been used to deduce relative atomic bond strengths and show that the icosahedra in boron carbide are not as stable as anticipated. Combined with quantum mechanics simulations, this result provides insight into the structural instability and amorphization of boron carbide. The temporal, spatial, and compositional information provided by atom probe tomography makes it a unique platform for elucidating the relative stability and interactions of primary building blocks in hierarchically crystalline materials.

bond dissociation | laser-assisted atom probe tomography | ab initio molecular dynamics | multiple hits

Icosahedra are commonly observed polyhedra in nature and can be found in a wide variety of molecules, viruses, minerals, and ceramics (1–4). The architecturally efficient icosahedral geometry and tight covalent bonding result in an unusually stable atomic configuration and in many cases, extraordinary properties. The prodigious structural stability, rigidity, and strength of C_{60} nearly spherical fullerene molecules (Bucky balls) are well-documented and have received considerable attention (5). Elemental boron and boron-based ceramics also form nearly spherical icosahedra (3, 4, 6), and the extreme hardness of these borides has been attributed to the presence of these icosahedra. In the case of boron carbide, one of the hardest structural ceramics, B_{12} or $B_{11}C$ icosahedra are stacked with rhombohedral symmetry and connected by three atom chains (Fig. 1*A*) (3, 6).

For boron carbide, the relative bond strength between the atoms in the icosahedra and chains is still being debated, but the icosahedra are generally thought to be very strong and stable because of their near-spherical shape and the highly delocalized fullerene-like intraicosahedral sp^2 bonds (3, 7–10). As a result of its high hardness, boron carbide is an excellent candidate for use in personal body armor; however, it undergoes a dramatic loss of ballistic performance in high-energy impacts. This loss is attributed to the formation of nanoscale amorphous shear bands (11). The shear amorphization of boron carbide has been confirmed by indentation experiments (12–16), but a fundamental understanding of the mechanism underlying it has not been fully established. It has been suggested that local shear first breaks the weaker chains and then, displaces and ruptures the stronger icosahedra (16), but recent quantum mechanics (QM) simulations attribute the instability to disintegration of the icosahedra (17, 18).

In this study, we carried out field evaporation experiments on boron carbide using a state of the art UV laser-assisted local electrode atom probe. Atom probe tomography (APT) is conventionally used for both 3D imaging and chemical composition measurements at the atomic scale (19, 20). Here, we embraced another dimension of atom probe data mining by statistically investigating the evaporation events, counting the types and numbers of atoms per laser pulse and deducing the relative stability of boron carbide icosahedra and chains. Our atom probe results show that, in boron carbide, the icosahedra are actually less stable than the chains and that chain–icosahedron bonds are unexpectedly strong, findings in direct contrast to conventional conjecture.

To carry out the field evaporation experiments, we shaped consolidated boron carbide samples with close to B_4C stoichiometry into very sharp needles with ∼20-nm radius using a focused ion beam (FIB). An example of an APT needle is provided in the bright-field transmission EM (TEM) micrograph in Fig. 1*B*. One common concern of using FIB-prepared specimens for APT data analysis is the structural and chemical changes induced by the high-energy Ga^+ beam (21). Boron and carbon were found to be uniformly distributed throughout the specimens, whereas gallium was only observed in the top few nanometers of each specimen (Fig. 1*C*). This result establishes that analyzed volumes taken away from the damaged layer are free of gallium implantation and that the detected field evaporation behavior is from the pristine boron carbide.

The atom probe experiments are conducted under the principles of field evaporation. Application of a very intense electric field polarizes surface atoms (or molecules), and superposition of rapid voltage or laser pulses ionizes and liberates individual atoms or molecules from the surface. The liberated ion is then accelerated by the intense electric field and captured on a position-sensitive detector that records its spatial and chemical information. Successive field evaporation events are used to create a 3D dataset of the sample (22). Details about the principles of APT can be found in *SI Materials and Methods*.

Significance

The extraordinary hardness of boron compounds is related to their internal structure, which is comprised of 12-atom icosahedra arranged in crystalline lattices. In these hierarchical materials, the icosahedra are easy to image with EM, but individual atoms are not. Here, we show that laser-assisted atom probe tomography can be used to deduce the atomic structure and relative interatomic bond strengths of atoms in boron carbide. To our surprise, the icosahedra disintegrated during the field evaporation process. Statistical analyses of event multiplicity and stoichiometry in the atom probe dataset substantiate that the icosahedra are less tightly bound than their interconnecting chains. Comparisons with quantum mechanics simulations further suggest that this instability plays a role in the amorphization of boron carbide.

Author contributions: K.Y.X., J.M.C., and K.J.H. designed research; K.Y.X., Q.A., T.S., and A.J.B. performed research; K.Y.X., Q.A., T.S., A.J.B., W.A.G., J.M.C., and K.J.H. analyzed data; and K.Y.X., Q.A., T.S., A.J.B., S.P.R., W.A.G., J.M.C., and K.J.H. wrote the paper.

The authors declare no conflict of interest.

This article is a PNAS Direct Submission.

[1]To whom correspondence should be addressed. Email: hemker@jhu.edu.

This article contains supporting information online at www.pnas.org/lookup/suppl/doi:10.1073/pnas.1607980113/-/DCSupplemental.

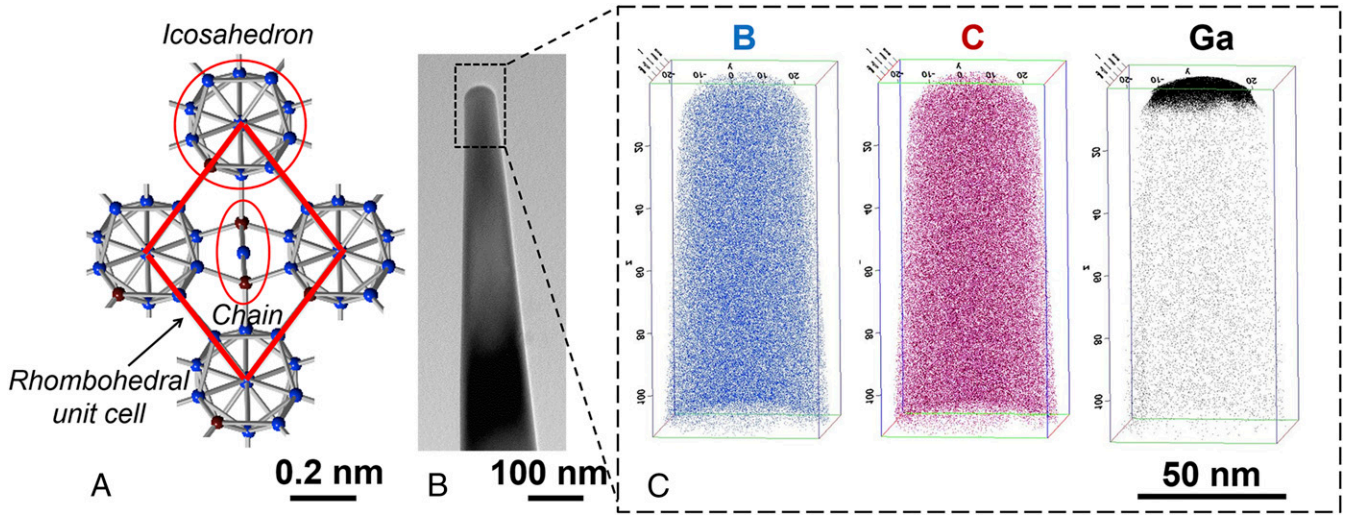

Fig. 1. (*A*) Crystal structure of boron carbide. (*B*) Bright-field TEM image of a boron carbide atom probe tip. (*C*) 3D atomic boron, carbon, and gallium maps of the atom probe tip.

Results and Discussion

During the laser-assisted field evaporation process, laser illumination provides thermal energy to the atom probe tip to assist in the field evaporation process. A pertinent question is whether the tip is melted by the laser pulse, but the dataset that we collected provides strong evidence to show that boron carbide tips

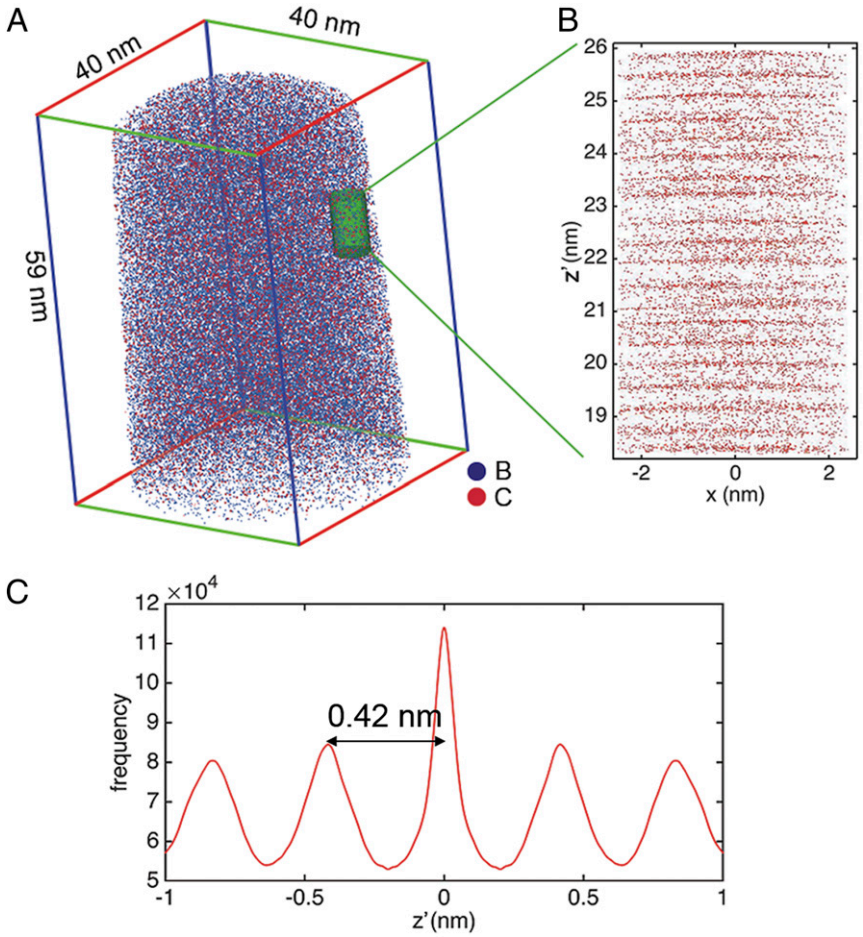

Fig. 2. Crystallographic information highlighted within the boron carbide atom probe dataset. (*A*) Boron carbide reconstruction with the region of interest shown in the green cylinder. (*B*) Clear evidence of (001) lattice planes in boron carbide. (*C*) 1D spatial map taken normal to the detected lattice planes showing peak to peak distances that correspond to the planar spacing of rhombohedral boron carbide.

do not melt during field evaporation. A detailed discussion of the thermal effects that occur during laser illumination can be found in *SI Materials and Methods* and Fig. S1, but the definitive evidence against melting is in the fact that we observed no loss of molecular-level crystallinity. The rhombohedral symmetry was retained (for example, Fig. 2), and (001) planes with a lattice spacing of 0.42 nm can be observed. This crystallinity provides clear evidence that the observed breaking of icosahedra in APT is not associated with high-temperature melting and opens an avenue for atomic-level characterization of the icosahedra.

The field evaporation characteristics of boron carbide in the atom probe can first be reasoned in a thought experiment. The icosahedra were expected to be very stable, and the intense electric field, assisted by laser-pulsed illumination, was expected to break the intericosahedral and chain–icosahedra bonds, with whole icosahedra evaporated as molecular ions. QM calculations (17, 18) predict that the most stable atomic configuration for crystalline boron carbide is $(B_{11}C)CBC$, with 12 atoms ($B_{11}C$) in each icosahedron and three atoms (CBC) in the chain. This configuration is supported but not yet confirmed by aberration-corrected scanning transmission electron microscopy (STEM) images (16). This APT study was originally undertaken to experimentally differentiate between the existence of $B_{11}C$ and B_{12} icosahedra. In the atom probe data, the peaks corresponding to $B_{11}C$ icosahedra on the mass spectrum would appear at about 130, 65, and 44 Da for charge states of 1+, 2+, and 3+, respectively.

To our surprise, APT experiments showed no such signals (Fig. 3*A*). All measured peaks have a mass to charge ratio of less than 25 Da. An expanded view of these peaks (Fig. 3*B*) reveals that they are predominantly boron and carbon ions, with a very small number (~0.3%) of C_2^+ complex ions. The icosahedra were completely disintegrated during field evaporation in the atom probe. This finding was consistent for all six tested specimens and insensitive to crystal orientation, direct current (DC) voltage (4–8 kV), specimen temperature (20–50 K), and laser energy (30–50 pJ) (Fig. S2).

Furthermore, closer examination of the evaporation statistics revealed that icosahedra and chains in boron carbide were field evaporated differently. In this study, ~35% of the atoms were detected as single events, and ~65% of the atoms were detected as multiple events (bar chart in Fig. 3*C*). Single events corresponded to the release of individual atoms, whereas a multiple event occurred when two or more atoms were liberated per laser pulse (23). Multiple events can be further partitioned into double events, triple events, etc. depending on the exact number of atoms detected per laser pulse. When the atomic fractions of boron and

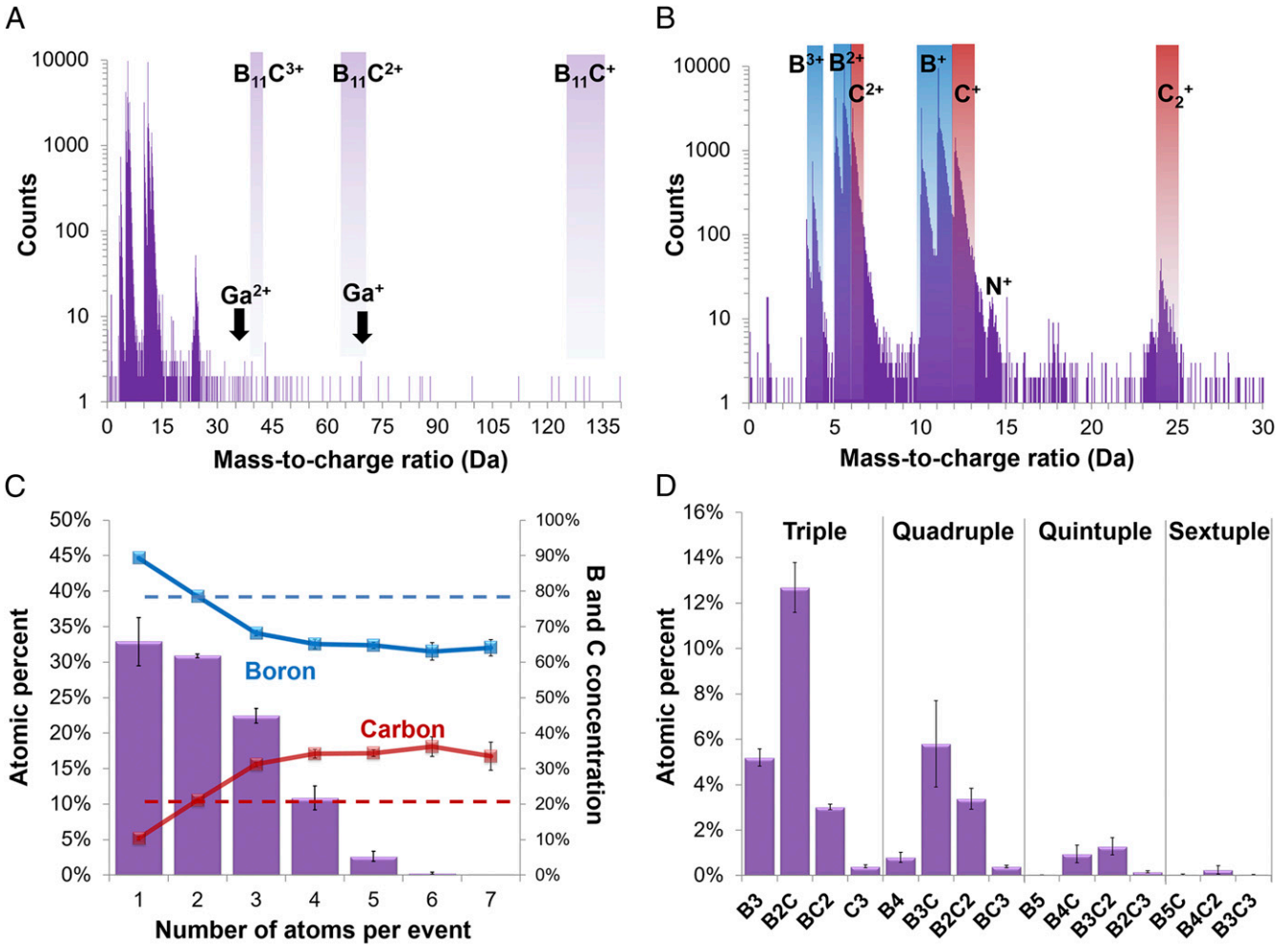

Fig. 3. (*A*) A typical mass spectrum of boron carbide produced with UV laser pulses. The purple swatches at m/q = 130, 65, and 44 indicate where signals from $B_{11}C$ icosahedra would have been but are absent. Note that the dataset is free from gallium damage. (*B*) Zoomed in view of *A* showing that most boron and carbon atoms were detected as individual ions. (*C*) Atomic composition of single and multiple events. Single events are boron-rich and result from icosahedra, whereas multiple events are carbon-rich and associated with chains. Dashed lines indicate the measured bulk composition. (*D*) Chemical correlation statistics of multiple events highlight the role of icosahedral–chain interactions.

carbon were plotted as a function of event multiplicity (solid lines with squares in Fig. 3*C*), they were found to be different and deviate from the bulk composition (dashed lines in Fig. 3*C*). The measured boron content in the single events is ~89%, very close to the $B_{11}C$ icosahedron stoichiometry of 92%. This correlation suggests that most of the single events can be attributed to atoms from the icosahedra. In the case of double events, the boron and carbon contents match the bulk composition, suggesting that equal proportions of icosahedra and chains were field evaporated. In higher-multiplicity events, the corresponding carbon concentrations are ~35%, much higher than the icosahedral carbon content of ~8%, suggesting that the higher-order multiple events involve atoms from the carbon-rich chains. As explained in *SI Materials and Methods*, this increase is not associated with multiple event-related detector dead time. This ~35% carbon concentration is significantly lower than that of CBC chains (at 67%), implying that some fragmented icosahedra were also evaporated in this scenario, which will be discussed shortly.

The apparent distinctions in the field evaporation behaviors of icosahedra and chains provide a direct comparison of their stabilities. The APT community has shown that atoms that are comparatively weakly bonded (e.g., metals) are more often evaporated as single events, whereas strongly bonded atoms (e.g., ceramics and polymers) tend to generate substantial numbers of complex ions and multiple events (22–25). We also note that most atoms detected in each multiple event were observed to be spatially correlated on the detector plane (Fig. S3), implying that the atoms that evaporated in a single laser pulse came from the same region of the sample and were originally bonded together (Fig. S4). In this series of experiments, most single events are attributed to the icosahedra, with multiple events associated with chains. This finding suggests that, contrary to common belief, the icosahedra are actually less atomically stable than the chains.

More detailed analysis of the chemical correlation (i.e., the statistics of atom species evaporated from each pulse in multiple events) offers additional insight on the relative instability of icosahedra. Inspection shows that most multiple events involve carbon atoms and that many involve more than one carbon atom (Fig. 3*D*). Events with multiple carbon atoms cannot come from a single icosahedron. Moreover, events with multiples of both boron and carbon (e.g., 2B2C, 3B2C, and 2B3C) could not have been produced by evaporation of a single chain or a single icosahedron. Coevaporation of neighboring icosahedra could, in principle, produce counts with two C atoms, but the overall stoichiometry of multiple atom events (Fig. 3*C*) does not support this interpretation. Instead, the observed chemical correlation indicates that portions of a chain and an adjacent icosahedron evaporate simultaneously, which points to the existence of strong chain–icosahedra bonding in boron carbide.

To further understand the destruction process of icosahedra in APT, we emulated field evaporation with QM simulations [Perdew–Burke–Ernzerhof (PBE) flavor of Density Functional Theory] using the Vienna ab initio simulation package (26, 27), which allowed visualization of the bond-breaking sequence and determination of the relative stability of the icosahedra and chains (Movie S1). To mimic the atom probe experiment in a simplified model, we created the (111) surface of the B_4C crystal, so that intact icosahedra might be most easily achieved. Other orientations [for example, (100)] tend to result in broken icosahedra on the surface, so that the stability of intact icosahedra cannot be directly assessed. To charge the surface atoms with broken bonds, we removed four electrons from the system. To mimic the high DC voltage on the specimen in the experiment, we applied a strong electric field 30 V/Å (28) perpendicular to the surface. Because laser illumination is fundamentally a thermally assisted process (29), we introduced thermal perturbations by heating the tip from 300 to 2,050 K over 8 ps. We note that the simulation requires an overestimation of the temperature expected in experiments because of the extremely small simulation cell and extremely high heating rate. Nevertheless, the QM simulations were used to gain insight into local bonding and its influence on the measured instability of the icosahedra.

The QM simulations cannot reproduce the ejection of ions from the surface, but they do provide an opportunity to monitor the evolution of local bonding and its effect on the arrangement of atoms both within and between neighboring icosahedra and chains. The ground-state structure of the (111) surface at 300 K is shown in Fig. 4*A*. All icosahedra (labeled 1–3) are intact, and the surface carbon atom (C) in the chain that was cut to create the surface stays connected to boron atoms (B_1 and B_2) in neighboring icosahedra. As the energy was increased, numerous intraicosahedral bonds in icosahedron 2 were broken, but atom C remained attached to atoms B_1 and B_2 (Fig. 4*B*). The observation that the intraicosahedral bonds were the first to break mimics our experimental finding that icosahedra were destroyed before they could be ionized and ejected from the surface. Both experiments and simulations indicate that, although icosahedra have strong sp^2 bonds and near-spherical geometry, they are not as stable as previously anticipated. By contrast, the chain–icosahedral interaction was found to be surprisingly stable. It is worth noting that icosahedra 1 and 3 remained intact when icosahedron 2 was broken, which further supports our interpretation that the breaking of icosahedra is caused by local interactions. Increasing the energy further provided additional insight on which chemical species may be liberated from the specimen surface. When icosahedra 1 and 2 were broken (Fig. 4 *C* and *D*), species, such as B2 and B2C, were released and are responsible for the multiple hit events that were recorded in the APT dataset (Fig. 3*D*). The QM simulations further suggest that, even at the highest energies, the icosahedra break sequentially, which can be used to explain the well-defined crystal lattice

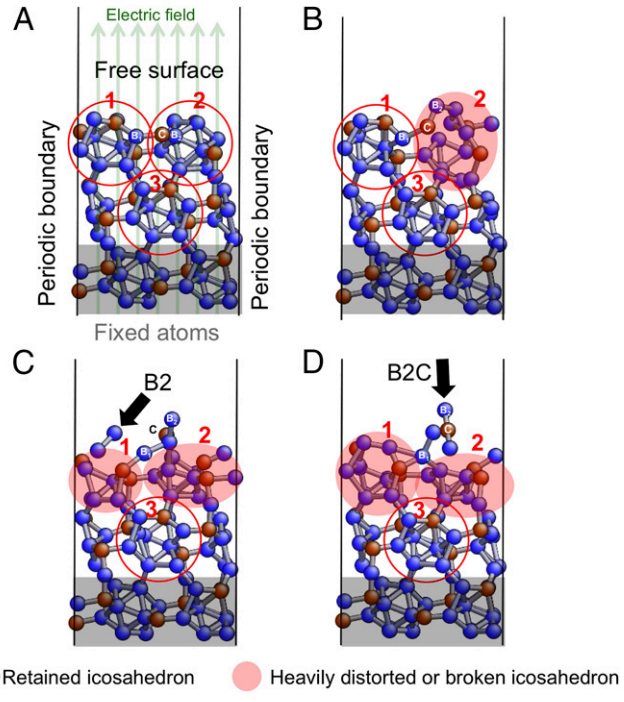

Fig. 4. The structural evolution of surface boron carbide icosahedra and chains at (*A*) the ground state, (*B*) a higher applied energy state, where one icosahedron starts to disintegrate, and (*C* and *D*) even higher applied energy states, where small molecular species can detach from the surface. Solid lines indicate the periodic boundaries, and shaded atoms in the bottom layer serve as the fixed boundary.

information in the acquired atom probe data (Fig. 2). To further examine the relative stability of the icosahedron and chain, we constructed a slab model with a surface icosahedron and an exposed C-B chain fragment and computed the minimum energy to extract a B-C diatomic unit from both the surface chain and the icosahedron (Fig. S5). The details of these calculations are described in *SI Materials and Methods*, and the results indicate that the required extraction energy for the surface chain is greater than for the surface icosahedron: 12.15 vs. 9.18 eV. This finding is consistent with our APT experiments evidencing that the icosahedra fragment easier than the chains.

Conclusions

In summary, the combination of atom probe experiments and QM simulation provides unique insight into the structural stability of boron carbide. Here, we show that the icosahedra in boron carbide are not as stable as previously anticipated and that the chain–icosahedron bonds are stronger than expected, which corroborates the hypothesis suggested by previous QM simulations that chain–icosahedra interactions trigger shear amorphization (17). This observation provides a key to understanding amorphization and the loss of ballistic performance in boron carbide. Furthermore, investigating the evaporation statistics using APT allowed us to conduct a characterization of the relative stability and the interactions of icosahedra and chains in boron carbide. This approach can be applied to directly compare the structural stability and chemical bond strengths of the building blocks in other hierarchical materials as well.

ACKNOWLEDGMENTS. We acknowledge the facilities and the scientific and technical assistance of the Australian Microscopy and Microanalysis Research Facility at the Australian Centre for Microscopy and Microanalysis, University of Sydney. This research was sponsored by the Army Research Laboratory and accomplished under Cooperative Agreement W911NF-12-2-0022. In addition, Q.A. and W.A.G. received partial support from Defense Advanced Research Projects Agency Grant W31P4Q-13-1-0010 (Program Manager John Paschkewitz) and National Science Foundation Grant DMR-1436985.

1. Hoffmann R, Lipscomb WN (1962) Theory of polyhedral molecules. I. Physical factorizations of the secular equation. *J Chem Phys* 36(8):2179–2189.
2. Zandi R, Reguera D, Bruinsma RF, Gelbart WM, Rudnick J (2004) Origin of icosahedral symmetry in viruses. *Proc Natl Acad Sci USA* 101(44):15556–15560.
3. Lazzari R, Vast N, Besson J, Baroni S, Dal Corso A (1999) Atomic structure and vibrational properties of icosahedral B 4 C boron carbide. *Phys Rev Lett* 83(16):3230–3233.
4. Hubert H, et al. (1998) Icosahedral packing of B12 icosahedra in boron suboxide (B6O). *Nature* 391(6665):376–378.
5. Krätschmer W, Lamb LD, Fostiropoulos K, Huffman DR (1990) C60: A new form of carbon. *Nature* 347(6291):354–358.
6. Clark H, Hoard J (1943) The crystal structure of boron carbide. *J Am Chem Soc* 65(11): 2115–2119.
7. Domnich V, Reynaud S, Haber RA, Chhowalla M (2011) Boron carbide: Structure, properties, and stability under stress. *J Am Ceram Soc* 94(11):3605–3628.
8. Kirfel A, Gupta A, Will G (1979) The nature of the chemical bonding in boron carbide, b13c2. I. Structure refinement. *Acta Crystallogr B* 35(5):1052–1059.
9. Kwei GH, Morosin B (1996) Structures of the boron-rich boron carbides from neutron powder diffraction: Implications for the nature of the inter-icosahedral chains. *J Phys Chem* 100(19):8031–8039.
10. Vast N, Lazzari R, Besson J, Baroni S, Dal Corso A (2000) Atomic structure and vibrational properties of icosahedral α-boron and B4C boron carbide. *Comput Mater Sci* 17(2):127–132.
11. Chen M, McCauley JW, Hemker KJ (2003) Shock-induced localized amorphization in boron carbide. *Science* 299(5612):1563–1566.
12. Domnich V, Gogotsi Y, Trenary M, Tanaka T (2002) Nanoindentation and Raman spectroscopy studies of boron carbide single crystals. *Appl Phys Lett* 81(20): 3783–3785.
13. Yan X, Li W, Goto T, Chen M (2006) Raman spectroscopy of pressure-induced amorphous boron carbide. *Appl Phys Lett* 88(13):131903–131905.
14. Ge D, Domnich V, Juliano T, Stach E, Gogotsi Y (2004) Structural damage in boron carbide under contact loading. *Acta Mater* 52(13):3921–3927.
15. Ghosh D, Subhash G, Sudarshan TS, Radhakrishnan R, Gao XL (2007) Dynamic indentation response of fine-grained boron carbide. *J Am Ceram Soc* 90(6):1850–1857.
16. Reddy KM, Liu P, Hirata A, Fujita T, Chen MW (2013) Atomic structure of amorphous shear bands in boron carbide. *Nat Commun* 4:2483.
17. An Q, Goddard WA, 3rd, Cheng T (2014) Atomistic explanation of shear-induced amorphous band formation in boron carbide. *Phys Rev Lett* 113(9):095501.
18. Fanchini G, McCauley JW, Chhowalla M (2006) Behavior of disordered boron carbide under stress. *Phys Rev Lett* 97(3):035502.
19. Kelly TF, Miller MK (2007) Invited review article: Atom probe tomography. *Rev Sci Instrum* 78(3):031101.
20. Moody MP, Vella A, Gerstl SS, Bagot PA (2016) Advances in atom probe tomography instrumentation: Implications for materials research. *MRS Bull* 41(01):40–45.
21. Felfer PJ, Alam T, Ringer SP, Cairney JM (2012) A reproducible method for damage-free site-specific preparation of atom probe tips from interfaces. *Microsc Res Tech* 75(4):484–491.
22. Müller EW, Panitz JA, McLane SB (1968) The atom-probe field ion microscope. *Rev Sci Instrum* 39(1):83–86.
23. Yao L, Gault B, Cairney J, Ringer S (2010) On the multiplicity of field evaporation events in atom probe: A new dimension to the analysis of mass spectra. *Philos Mag Lett* 90(2):121–129.
24. Hono K, et al. (2011) Broadening the applications of the atom probe technique by ultraviolet femtosecond laser. *Ultramicroscopy* 111(6):576–583.
25. Tsong T (1984) Pulsed-laser-stimulated field ion emission from metal and semiconductor surfaces: A time-of-flight study of the formation of atomic, molecular, and cluster ions. *Phys Rev B* 30(9):4946–4961.
26. Kresse G, Hafner J (1993) Ab initio molecular dynamics for liquid metals. *Phys Rev B* 47(1):558–561.
27. Kresse G, Furthmüller J (1996) Efficient iterative schemes for ab initio total-energy calculations using a plane-wave basis set. *Phys Rev B* 54(16):11169–11186.
28. Gault B, Moody MP, Cairney JM, Ringer SP (2012) *Atom Probe Microscopy* (Springer Science & Business Media, New York).
29. Cerezo A, Smith G, Clifton P (2006) Measurement of temperature rises in the femtosecond laser pulsed three-dimensional atom probe. *Appl Phys Lett* 88(15):154103.
30. Breen AJ, et al. (2015) Restoring the lattice of Si-based atom probe reconstructions for enhanced information on dopant positioning. *Ultramicroscopy* 159(Pt 2):314–323.
31. Kellogg G, Tsong T (1980) Pulsed-laser atom-probe field-ion microscopy. *J Appl Phys* 51(2):1184–1193.
32. Gault B, et al. (2006) Design of a femtosecond laser assisted tomographic atom probe. *Rev Sci Instrum* 77(4):043705.
33. Liu H, Liu H, Tsong T (1986) Numerical calculation of the temperature distribution and evolution of the field-ion emitter under pulsed and continuous-wave laser irradiation. *J Appl Phys* 59(4):1334–1340.
34. Marquis EA, Gault B (2008) Determination of the tip temperature in laser assisted atom-probe tomography using charge state distributions. *J Appl Phys* 104(8):084914.
35. Liu H, Tsong T (1984) Numerical calculation of the temperature evolution and profile of the field ion emitter in the pulsed-laser time-of-flight atom probe. *Rev Sci Instrum* 55(11):1779–1784.
36. Du S, et al. (2013) Quantitative dopant distributions in GaAs nanowires using atom probe tomography. *Ultramicroscopy* 132:186–192.
37. Du S, et al. (2013) Full tip imaging in atom probe tomography. *Ultramicroscopy* 124: 96–101.
38. Meisenkothen F, Steel EB, Prosa TJ, Henry KT, Prakash Kolli R (2015) Effects of detector dead-time on quantitative analyses involving boron and multi-hit detection events in atom probe tomography. *Ultramicroscopy* 159(Pt 1):101–111.
39. Müller M, Saxey DW, Smith GD, Gault B (2011) Some aspects of the field evaporation behaviour of GaSb. *Ultramicroscopy* 111(6):487–492.
40. Yao L, Cairney J, Gault B, Zhu C, Ringer S (2013) Correlating spatial, temporal and chemical information in atom probe data: New insights from multiple evaporation in microalloyed steels. *Philos Mag Lett* 93(5):299–306.
41. Saxey DW (2011) Correlated ion analysis and the interpretation of atom probe mass spectra. *Ultramicroscopy* 111(6):473–479.
42. La Fontaine A, et al. (2015) Interpreting atom probe data from chromium oxide scales. *Ultramicroscopy* 159(Pt 2):354–359.